SRI International

Final Report • 15 January 1998

THEORY OF INDIUM THALLIUM PHOSPHIDE

Prepared by:

S. Krishnamurthy, Senior Research Physicist
Applied Physical Sciences Laboratory

SRI Project 6457

Prepared for:

Air Force Office of Scientific Research — AFOSR/NE
Directorate of Physics and Electronics
110 Duncan Avenue, Suite B115
Bolling Air Force Base, DC 20332-0001

Attn: Mike Prairie, Program Manager

Contract F49620-95-C-0010

CDRL 0002AC

Approved:

Elizabeth J. Brackmann, Co-Director
Applied Physical Sciences Laboratory

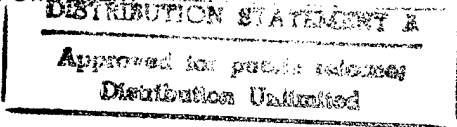19980129 055

DTIC QUALITY INSPECTED 2

REPORT DOCUMENTATION PAGE

Public reporting burden for this collection of information is estimated to average 1 hour per response, including the time for reviewing instructions, searching existing data sources, gathering and maintaining the data needed, and completing and reviewing the collection of information. Send comments regarding this burden estimate or any other aspect of this collection of information, including suggestions for reducing this burden, to Washington Headquarters Services, Directorate for Information Operations and Reports, 1215 Jefferson Davis Highway, Suite 1204, Arlington, VA 22202-4302, and to the Office of Management and Budget, Paperwork Reduction Project (0704-0188), Washington, DC 20503.

1. AGENCY USE ONLY (Leave Blank)	2. REPORT DATE	3. REPORT TYPE AND DATES COVERED
		Final Technical Report

4. TITLE AND SUBTITLE
THEORY OF INDIUM THALLIUM PHOSPHIDE

5. FUNDING NUMBERS
6110 3 F
2 3 0 5 /FS

6. AUTHOR(S)
S. Krishnamurthy

7. PERFORMING ORGANIZATION NAME(S) AND ADDRESS(ES)

SRI International
333 Ravenswood Avenue
Menlo Park, CA 94025

8. PERFORMING ORGANIZATION REPORT NUMBER
6457FR

9. SPONSORING/MONITORING AGENCY NAME(S) AND ADDRESS(ES)
Air Force Office of Scientific Research—AFOSR/NE
Directorate of Physics and Electronics
110 Duncan Avenue, Suite B115
Bolling Air Force Base, DC 20332-0001

10. SPONSORING/MONITORING AGENCY REPORT NUMBER
F49620-95-C-0010

11. SUPPLEMENTARY NOTES

12a. DISTRIBUTION/AVAILABILITY STATEMENT

12b. DISTRIBUTION CODE

13. ABSTRACT (Maximum 200 words)
We have used a combination of first principles and empirical band structures to study various properties of new classes of IR materials, the III-V alloys In(1-x)TlxQ, where Q=P, As, or Sb: temperature variation of the band gap, absorption coefficient, minority carrier lifetimes, thermodynamic phase diagram, low-field electron and hole mobilities, native point defect (such as vacancies and antisites) concentrations, parameters needed for modeling MBE growth.

We found that, in the case of the LWIR InTlP alloy, the band gap increases with temperature, growth requires very high P vapor pressures, the electron mobility and absorption coefficients are comparable to those of LWIR HgCdTe, and the minority carrier lifetimes are about one-third of that in HgCdTe. The overall conclusion is that InTlP has serious growth-related problems that can be overcome only with novel nonequilibrium growth methods or high pressure LPE growth.

InTlAs is a more promising candidate to be grown because the Tl concentration needed to attain an LWIR response is lower and the vapor pressure needed to grow it is also much lower. Moreover its Auger lifetime is predicted to be about a factor of 10 larger than that of HgCdTe.

14. SUBJECT TERMS
InTlP, InTlAs, InTlSb, III-V IR material, band structures, phonons, band gap variation, absorption coefficient, minority carrier lifetimes, phase diagram, defect density, modeling MBE growth, electron mobility, Auger rates

15. NUMBER OF PAGES

16. PRICE CODE

17. SECURITY CLASSIFICATION OF REPORT	18. SECURITY CLASSIFICATION OF THIS PAGE	19. SECURITY CLASSIFICATION OF ABSTRACT	20. LIMITATION OF ABSTRACT
UNCLASSIFIED	UNCLASSIFIED	UNCLASSIFIED	UNLIMITED

CONTENTS

LIST OF ILLUSTRATIONS

LIST OF TABLES

LIST OF ABBREVIATIONS

BZ	Brillouin zone
FD	Fermi-Dirac
FPA	focal plane array
GQCA	generalized quasi-chemical approximation
GSMBE	gas source molecular beam epitaxy
HPTB	hybrid pseudopotential tight-binding
IR	infrared
IRFPA	infrared focal plane array
LDA	local density approximation
LMTO	linearized muffin-tin orbital
LO	longitudinal optical
LPE	liquid phase epitaxy
LWIR	long wave infrared
MBE	molecular beam epitaxy
MOCVD	metal-organic chemical vapor disposition
MOMBE	metal-organic molecular beam epitaxy
MWIR	mid wave infrared
ROIC	read out integrated circuits
TB	tight-binding
VLWIR	very long wave infrared

PREFACE

This report summarizes the work accomplished during the period 15 November 1994 through 14 November 1997, under the AFOSR Contract F49620-95-C-0010 entitled, "Theory of InTlP."

1 INTRODUCTION

$Hg_{0.78}Cd_{0.22}Te$, InSb, and other materials used or proposed for use in infrared focal plane arrays (IRFPA) are highly developed, with some functioning well enough to meet current system requirements. However, at present all are imperfect and exhibit one or more performance limiting traits (Sher et al., 1991) that prevent them from meeting the most stringent current system specifications; and in their present state they cannot meet requirements foreseen for future systems. It is not certain if $Hg_{0.78}Cd_{0.22}Te$ can be improved to a point where it will meet these future requirements (e.g., much lower costs, higher operating temperatures, multispectral response, larger arrays, etc.).

For years, researchers have sought a III-V compound or group IV-based material capable of responding in the long-wave infrared (LWIR). The motivator for the search was the general fact that these materials might have better materials properties than II-VI-based alloys. The alloys GeSn, SiSn, and InSbBi have been suggested and tried (Zelko and Green, 1978; Levine et al., 1991). However, solubility limits have caused these efforts to fail. The materials have been prepared by nonequilibrium-energy-assisted epitaxial growth methods, but these methods have never become practical.

III-V-based quantum well structure and strained layer superlattices are now being tried with some success, but they still suffer from poor quantum efficiencies (Osbourn et al., 1987). A few years ago, we suggested that $In_{1-x}Tl_xSb$ would be stable in the zinc-blende structure for $x < 0.15$, but would have to be grown by a vapor phase technique (metal-organic chemical vapor disposition [MOCVD] or molecular beam epitaxy [MBE]) because of phase-diagram-precluded liquid phase epitaxy (LPE) or bulk growth techniques (van Schilfgaarde and Sher, 1993). This occurs because TlSb forms in the CsCl structure. If it works, $x = 0.09$ would suffice to cause the alloy to respond to LWIR. Because this alloy is projected to have array processing conditions not differing greatly from InSb, we suggested that it could be processed on current InSb array manufacturing lines resulting in LWIR FPAs instead of mid wave IR (MWIR) with little extra investment required. However, even if this proves to be possible and even if essentially the same read out integrated circuits (ROIC) can be used, the In bonds between the FPA and ROIC would still limit array size.

Later on, we evaluated $In_{0.33}Tl_{0.67}P$ and $In_{0.85}Tl_{0.15}As$ for possible application in FPAs (van Schilfgaarde et al., 1993). Both are predicted to have structural and electrical properties superior to $Hg_{0.78}Cd_{0.22}Te$ for MWIR, LWIR, and very long wave IR (VLWIR) FPAs. However, $In_{0.33}Tl_{0.67}P$ has only a 2% lattice mismatch with InP, so InP can serve as a low dislocation density substrate material capable of supporting ICs for an integrated, on chip ROIC. This would remove one of the more serious limitations for the FPAs.

We studied $In_{0.33}Tl_{0.67}P$ in more detail and also assisted in the ongoing experimental work. Toward that end the objective of this effort focused on the following tasks:

- Task 1: Temperature variation of the band gap

- Task 2: Absorption coefficient

- Task 3: Auger lifetime

- Task 4: *n*- and *p*-type dopant levels and densities

- Task 5: Low-field electron and hole mobility

- Task 6: Native point defect (such as vacancies and antisites) concentration

- Task 7: Parameters needed for modeling MBE growth

- Task 8: Support of ongoing experiments.

We have successfully completed all these tasks. In place of Task 4, we have calculated the thermodynamical phase diagram which should be more useful to experimentalists in growing the alloys. The major results of our efforts are summarized herein; details can be found in various journal articles that resulted from this work.

2 BAND STRUCTURES

2.1 GENERAL

Studies of band structures of semiconductors and their alloys have been carried out extensively in the literature. The methods range from *ab initio* or first-principles approaches, where the single-particle Schrödinger equation is solved in a local density approximation (LDA), to empirical tight-binding (TB) approximations. While these methods are excellent for predicting structural and other ground state properties, the band gaps are systematically underestimated. In addition, these methods are often too complicated and time consuming to be included in realistic device modeling. Although one *ab initio* method, GW, has been demonstrated to get accurate gaps for semiconductors, the calculation is even more time consuming, making the comprehensive studies impractical.

Empirical TB methods are extremely fast and easy to use. In these methods the real-space matrix elements of the Hamiltonian are fit to experiments or first-principles predictions of the band structure at various symmetry points of the Brillouin zone (BZ). These Hamiltonians, along with an empirical model for the spatial variation of the matrix elements, have been used to study structural and electronic properties. The major disadvantages of the TB methods are their lack of (1) quantitative predictability, (2) band structures throughout the BZ, and (3) accurate wave functions. The information obtained by these methods can be used only to study trends.

Between these two extremes lay methods such as k·P, empirical pseudopotentials, semi-*ab initio*, and a hybrid pseudopotential tight-binding (HPTB) approach (Chen and Sher, 1995). These methods vary substantially in accuracy and computational time. They are semi-empirical in nature, but obtain good band structure with explicit wave functions.

In the HPTB method, the local sp^3 orbitals are expanded in plane waves and the interatomic matrix elements are obtained from empirical pseudopotentials. The Hamiltonian is then fine-tuned with the addition of a localized empirical tight-binding Hamiltonian to obtain correctly all observed band structure features.

In the absence of experimental information, as in the case of InTlP alloys, we rely on the trustworthy aspects of first-principles, LDA-based linearized muffin-tin orbital approximation (LMTO) band structures. The LDA Hamiltonians always predict gaps smaller than experiment. Following a simple theory (Harrison, 1980) the correction to the band gap U / ε_∞ is added. The coulombic repulsion U between the local excess charge and the excited electron is also calculated in LDA. With this correction, we estimate the uncertainty in the predicted gaps to be about 0.1 eV.

We carried out calculations similar to that of Chen and Sher (1995) for TlAs, TlP, and TlSb. These materials are predicted to have a negative band gap. Hence the gap in the alloys $In_xTl_{1-x}P$, $In_xTl_{1-x}As$, and $In_xTl_{1-x}SB$ can vary from 0 to 1.4 eV and consequently are potential candidates for infrared applications (van Schilfgaarde et al., 1993). A detailed survey including lattice mismatch, defect densities, and structural, transport and optical properties suggests that the Tl alloys can be good alternatives to $Hg_xCd_{1-x}Te$ alloys for LWIR FPAs (Sher et al., 1994). The details of the band structure methods and the parameters for the tight-binding Hamiltonian have been published by Krishnamurthy et al. (1997).

2.2 TEMPERATURE DEPENDENCE

The temperature (T) dependence of energy gaps of semiconductors is of great physical and technological interest. The variation in the gap is relatively large in small-gap materials and precise knowledge of the temperature dependence of the gaps is essential in device design. The quantities such as band offset and effective mass depend sensitively on the temperature variation of band edges. The gap decreases with increasing temperature in medium-gap and wide-gap semiconductors, and it increases in small-gap materials such as HgCdTe, PbS, PbSe, and PbTe. The thermal expansion of the lattice and electron–phonon interactions are usually considered causes for the temperature variation of the band structures. Thermal expansion always reduces gaps.

When the temperature of the lattice is increased, the lattice expands. This expansion, called dilation, decreases the bandgap. The number of phonons in the lattice increases with temperature. The change in potentials caused by the displacement of atoms from their equilibrium positions introduces an electron–phonon interaction. These interactions, viewed as a perturbation, will change the electronic states — that is, the band structure. A major contribution to the bandgap change with temperature arises from this interaction.

In a perturbation-theory treatment of electron–phonon interactions, the intraband transitions reduce the gap whereas interband transitions increase it; the net shift in the gap can be positive or negative. We calculated the gap variation starting from accurate band structures, wave functions, and proper phonon dispersion relations, taking into account matrix elements of the electron–phonon interactions. The contributions from each phonon branch to each electron band have been obtained to assist physical understanding of the underlying causes of the variations.

The electron acoustic phonon interactions are usually parameterized in terms of wave-vector- and energy-independent deformation potential coupling constants. Our calculations generalized the above approach considerably. We use accurate tight-binding band structures for electrons and the valence force field model for phonon bandstructures. A firm theoretical base has been established for the validity of this valance force field procedure. We include contributions from all six phonon modes, with wave vectors spanning the entire BZ.

Contrary to traditional thinking which is based on total density of states arguments, we showed that *both* conduction and valence band edges move down in energy. When the valence band edge moves more than the conduction band edge, the gap increases with T, as in the case of some $Hg_{1-x}Cd_xTe$ alloys with $x < 0.5$. The reverse occurs for all non-thallium-bearing III-V compounds studied, $Hg_{1-x}Cd_xTe$ alloys with $x < 0.5$, and most thallium alloys. One important consequence of this observation will be in the band offsets in semiconductor heterojunction devices. Interestingly, the gap is nearly constant with temperature in $In_{0.33}Tl_{0.67}P$. In addition to the gap, other features of the band structure change with temperature and will affect the spectral variations of the absorption coefficient and transport properties.

The details of these calculations and results on various semiconductors and alloys have been published (Krishnamurthy et al., 1995). These calculations of band gap variation with temperature are extended to thallium alloys. The results of our calculations carried out for $In_{0.33}Tl_{0.67}P$ and the competing LWIR material $Hg_{0.78}Cd_{0.22}Te$ alloys are shown in Figure 1. Note that the gap increases with temperature for both $In_{0.33}Tl_{0.67}P$ and $Hg_{0.78}Cd_{0.22}Te$. However, the rate of increase is almost zero for $In_{0.33}Tl_{0.67}P$ whereas it is substantial for $Hg_{0.78}Cd_{0.22}Te$. This predicts an added advantage for $In_{0.33}Tl_{0.67}P$ over $Hg_{0.78}Cd_{0.22}Te$ when they are used in IR detectors. The internal temperature of any device is bound to increase while in operation. The larger the dE_g/dT, the more severe are the requirements on the device design to maintain constant temperature profiles over the whole working area. When the changes in the gap are minimal, as in the case of $In_{0.33}Tl_{0.67}P$, detector and dewar design constraints are eased. The gap in InAs is known to decrease with temperature, and as $In_{0.85}Tl_{0.15}As$ is rich in InAs, the gap in $In_{0.85}Tl_{0.15}As$ follows a similar trend. However, the small slope also bodes well for $In_{0.85}Tl_{0.15}As$ devices.
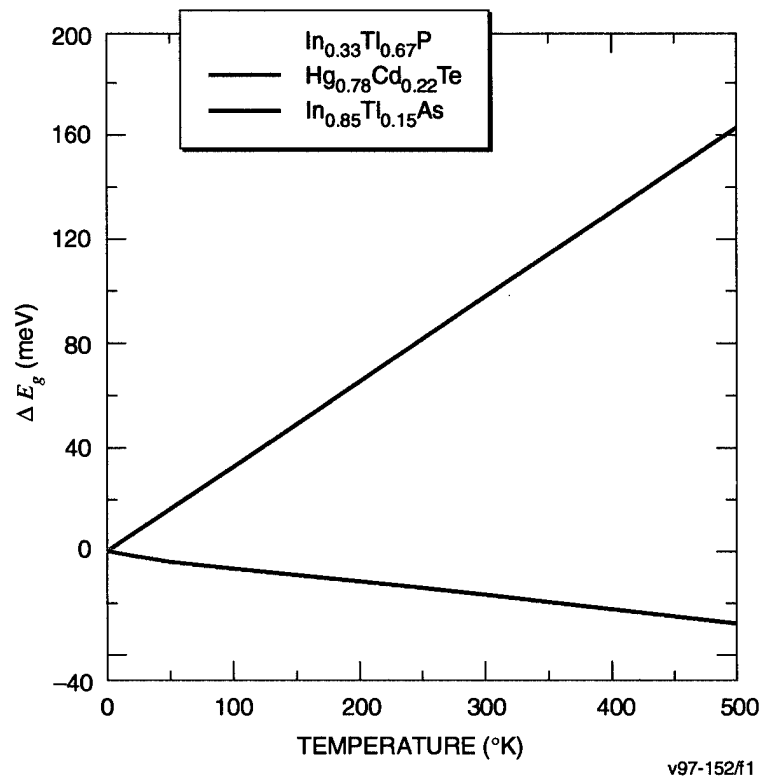
Figure 1   TEMPERATURE-DEPENDENT BAND GAPS

6

3 PHASE DIAGRAM

3.1 COMPOUNDS

We have evaluated thermodynamic factors that may impact the growth of the Tl-based compounds. We have calculated the equilibrium vapor pressures of the constituents over the solids throughout the existence region and as a function of alloy concentration. Calculations have been benchmarked against several systems for which experimental values are available. We find that the binaries are unstable with respect to decomposition into the elemental metals, thallium and phosphorous for TlP and thallium and arsenic for TlAs. Even with conservative estimates of the errors inherent in the LDA we conclude that the binaries will have no existence region. Details of this work are given in Berding et al. (1997).

3.2 ALLOYS

Thermodynamical factors that affect growth of the thallium-bearing zinc-blende alloys InTlP and InTlAs are examined within the LDA, using the LMTO method. The LDA predicts TlP and TlAs to be unstable with respect to decomposition into the elemental constituent solids, or marginally stable if conservative estimates of the LDA errors are made. Several thallium-rich and anion-rich compounds have also been examined; some are found to have excess energies per atom comparable to the zinc-blende phase. The equilibrium partial pressures over InTlP and InTlAs have also been calculated as a function of composition. Even with conservative error estimates, we predict that only low concentrations of thallium can be achieved in InTlP ($< 5\%$ at 350 °C) using gas source molecular beam epitaxy (GSMBE), far less than the 67% needed for LWIR applications. Although much less than 1% thallium is predicted to be soluble in InTlAs for GSMBE growth at 350 °C, the addition of error estimates into the calculation indicates that obtaining the 15% thallium needed for LWIR applications may be possible. Native defect populations have been calculated for alloy compositions corresponding to band gaps in the LWIR, and the anion antisite densities are predicted to be quite high, especially in InTlP, reflecting the comparable stability of the TlP and TlP_3 phases. The details of the calculations and results on the phase diagrams are published elsewhere (Berding et al., 1997); calculation of the defect properties are discussed in Appendix A.

LDA predicts the zinc-blende binaries TlP and TlAs to be unstable with respect to decomposition into the elemental solids, and both a Tl_7P_2 and a TlP_3 in the CuAu structure are shown to have comparable excess energies per atom to the zinc-blende TlP phase. The vapor pressures of the constituents over InTlP and InTlAs as a function of energies were calculated by using the local density approximation. Even if conservative error estimates are made, we predict that only very low concentrations of thallium will be achievable in the InTlP alloys ($< 0.1\%$), far

7

less than the 67% predicted to be necessary for band gaps in the LWIR. Although our calculations indicate that less than 1% thallium will be achievable in InTlAs, if conservative error estimates are made, the 15% needed for LWIR applications may be possible; there is also the possibility of growing LWIR InTlAs from the liquid. A preliminary examination of native point defects in $In_{0.33}Tl_{0.67}P$ and $In_{0.85}Tl_{0.15}As$ predicts that the anion antisite is the dominant defect and will be most troublesome in the InTlP. The high phosphorus antisite densities are indicative of the formation of the TlP_3 compound in the zinc-blende-based CuAu structure that we have found elsewhere to have an excess energy comparable to TlP.

4 MODELING GROWTH

The growth of HgTe in (100), (111)Hg, (111)Te, (211)Hg, and (211)Te orientations have been tried. It has been demonstrated that high quality HgTe growth, without formation of twin faults, can be obtained in the (211)Te orientation.

We carried out various energies required in a reliable modeling of growth of HgTe in (111), (110), (100), and (211) directions. From the calculated energies required to remove atoms from various configurations on (111), (110), (100), and (211) HgTe surfaces, excess pair energies are obtained. Those excess energies can be then used in a quasi-equilibrium thermodynamic or non-equilibrium Monte-Carlo growth models.

We obtained the energies using a Green's function method with full band structures. We develop a thermodynamic model to describe multilayer growth using effective excess pair energies and a generalized quasi-chemical approximation (GQCA). We use our calculated excess pair energies in a three bilayer model to study the critical temperature and island formation on (100), (111), (110), and (211) orientations. In order to get insight into vacancy segregation, we calculate the vacancy formation energy as functions of layer depth and surface orientations (Krishnamurthy et al., 1996a).

As InTlP alloys had never been grown, modeling was undertaken to aid growers in choosing proper conditions. The parameters needed for modeling are extracted from calculated sublimation energies of constituent species from various crystal orientations. We have found the growth rate, quality of growth, ratio of constitutional vapor pressures required to achieve stoichiometric growth, and defect densities depend sensitively on the choice of growth orientation of the substrate.

The calculated excess energies for intralayer anion–anion (e_1), cation–cation (e_2), anion–cation (ε_1) bonds, and for interlayer anion–cation (ε_2), cation–anion (ε_3) bonds are given in Table 1. The negative excess energy for a given bond implies that atom–vacancy pair is preferred to atom–atom pair. The surfaces that are shown with a critical temperature (T_c) undergo smooth to rough phase transition at T_c. When the net repulsive (negative) energies are stronger, the surfaces undergo order-disorder phase transitions, indicated here with asterisks. In the cases where smooth-to-rough transition exists, the calculated T_c are found to be considerably higher than the usual growth temperatures of the order of 300 °C, so the growth on these surfaces is expected to be layer-by-layer (two-dimensional) with the formation of islands. For surfaces with larger T_c, smaller grown-in defect densities are expected. A cation terminated (100) surface has the largest T_c. However, among the surfaces studied, the (211)A surface has the smallest

9

Table 1

EXCESS PAIR ENERGIES (in eV), ROUGHNESS TRANSITION TEMPERATURE (IN °C), AND ANION AND CATION SUBLIMATION (E_{SUB}) (IN eV)

Surface	e_1	e_2	ε_1	ε_2	ε_3	T_c	E_{sub}^a	E_{sub}^c
(211)A	0.38	0.34	0.30	0.27	−0.14	2273	−1.27	1.71
(211)B	0.27	0.16	0.76	1.36	0.73	2173	−1.87	3.75
(111)A	0.25	0.07	0.12	–	−0.59	3253	−2.37	1.48
(111)B	−0.09	0.03	−0.48	–	−1.01	*	−2.40	1.74
(100)A	0.34	0.09	0.75	–	−0.27	5373	−2.69	2.31
(100)B	0.09	0.34	−0.27	–	0.75	*	−2.69	2.31

* Stronger negative energies cause surface to undergo order-disorder phase transition

repulsive binding energy for P. (The final state for the evaporating P is considered to be P_2.) It implies that growth on this surface can be achieved with far less P over pressure than that needed, for example, on the (100) surface. In addition, the T_c for the (211)A surface is considerably large. These observations suggest that growth on (211)A offers a considerable advantage over other surfaces. In any case, it is clear that growth has to take place with a cation terminated surface with considerably large P over pressure to keep the P atoms in the epilayers.

5 TRANSPORT PROPERTIES—MOBILITY

The transport-related properties such as electron mobility, Hall coefficient, and Fermi levels are calculated with the accurate analytical band structures, Fermi-Dirac (FD) statistics, and the calculated energy gap. As the low-field mobility involves states close to the conduction band edge, we fit the conduction band accurately to an analytical function. In the small gap materials such as $In_{0.33}Tl_{0.67}P$ the hyperbolic function fits the conduction band (up to 0.5 eV from the band edge) extremely well. The error added due to this fitting procedure is usually less than 0.1%. However, these calculated values differ substantially from the ones obtained with effective mass or parabolic band structure approximations to $In_{0.33}Tl_{0.67}P$ alloy bands. As the gap is small, there will be substantial carriers in the conduction band requiring the use of FD statistics. The calculated Fermi level, number of dopants and intrinsic carriers are used to obtain a full solution to the Boltzmann transport equation (Krishnamurthy and Sher, 1995). Our calculated impurity, phonon, and alloy disorder-limited electron mobilities in $In_{0.33}Tl_{0.67}P$ and $Hg_{0.78}Cd_{0.22}Te$ are shown in Figure 2. Our calculations explain the observed hump in mobility in $Hg_{0.78}Cd_{0.22}Te$ without the need for postulating additional contribution mechanisms. Such a hump is not predicted in Tl alloys. Due to the larger phonon energies (38 meV in $In_{0.33}Tl_{0.67}P$ and 17 meV in $Hg_{0.78}Cd_{0.22}Te$), electron–phonon interactions are less effective in InTlP and consequently its mobility does not fall as rapidly with temperature and is larger above 100K than that of $Hg_{0.78}Cd_{0.22}Te$. At lower temperatures, the mobility in $Hg_{0.78}Cd_{0.22}Te$ is larger by a factor of 2 to 4. In any case, electron mobilities in both alloys are roughly 10^5 cm^2/V-sec.
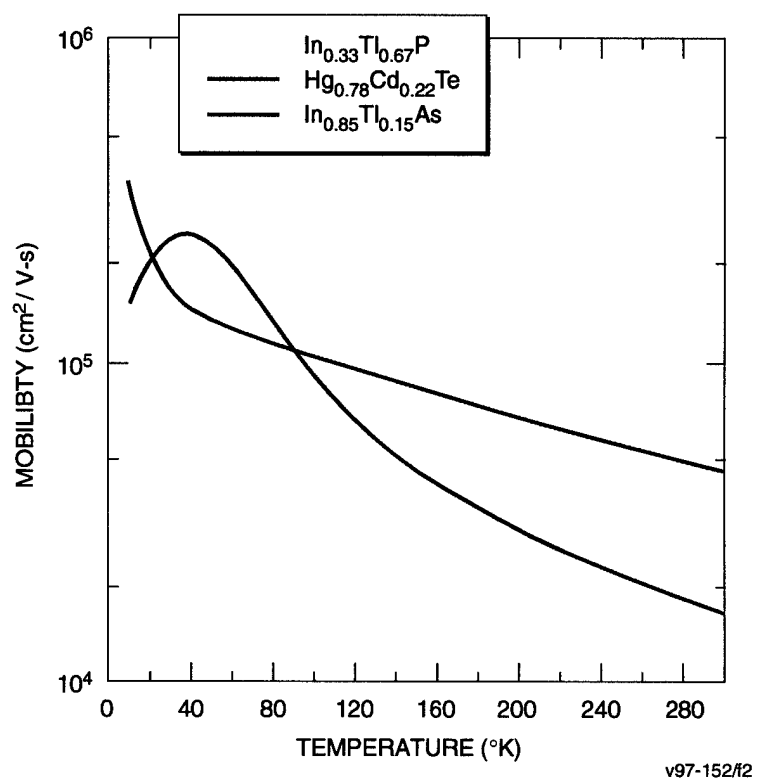
Figure 2 TEMPERATURE-DEPENDENT MOBILITIES

v97-152/f2

12

6 OPTICAL PROPERTIES—ABSORPTION

One of the important factors affecting the efficiency of IR devices is the near band edge absorption. All IR alloys have direct gaps. The intrinsic interband absorption coefficient should rise sharply at the band gap energy when the photon energy increases. This rate of increase with photon energy is one measure of the merit of a semiconductor for photodetector applications and hence plays a crucial role in determining the efficiency of the absorption devices. Our calculation of the absorption coefficient of these new Tl-based alloys will be useful in evaluating the suitability of these materials for IR applications.

We have calculated the absorption coefficient using full band structures by explicitly evaluating the momentum matrix elements from the wave functions and band structure states. To test the accuracy, first we carried out the calculation for GaAs for which several reliable experimental spectra are available for comparison. We found that our calculations are in good agreement with those experiments. The calculations were then extended to HgCdTe, InTlP, InTlAs, and InTlSb alloys at concentrations corresponding to 0.1 eV and 0.25 eV band gaps, respectively, for LW and MWIR applications. The method of approach and the calculation details have been published by Krishnamurthy et al. (1996b).

We considered the Tl-based alloys at the concentrations corresponding to a 0.1 eV band gap and compared them with those of GaAs and HgCdTe alloys. The calculated values of α in GaAs are shown by the light blue line in Figure 3. Also shown are the values of $Hg_{0.78}Cd_{0.22}Te$ (0.1 eV gap) and $Hg_{0.70}Cd_{0.30}Te$ (0.25 eV gap), $In_{0.67}Tl_{0.33}P$, $In_{0.92}Tl_{0.08}Sb$, and $In_{0.85}Tl_{0.15}As$. To enable better comparison, all curves are plotted as a function of $\hbar\omega - E_g$, where E_g is the band gap. The absorption over the extended energy range as shown in Figure 3 indicates that GaAs falls between better-absorbing HgCdTe and less-absorbing thallium alloys. However, IR applications and band gap estimation studies normally require information in the energy range that corresponds to α values of less than about 2000 cm^{-1}. For such a case, the near band edge absorption (typically with 20 meV from the conduction band edge) in GaAs, HgCdTe alloys, and InTlP alloys is about the same within the calculational accuracy, and that in InTlAs and InTlSb is weaker. The prediction which is based solely on the absorption parameter, is that the InTlP alloy will compare well with HgCdTe for LWIR applications, whereas the materials InTlAs and InTlSb are less favorable.
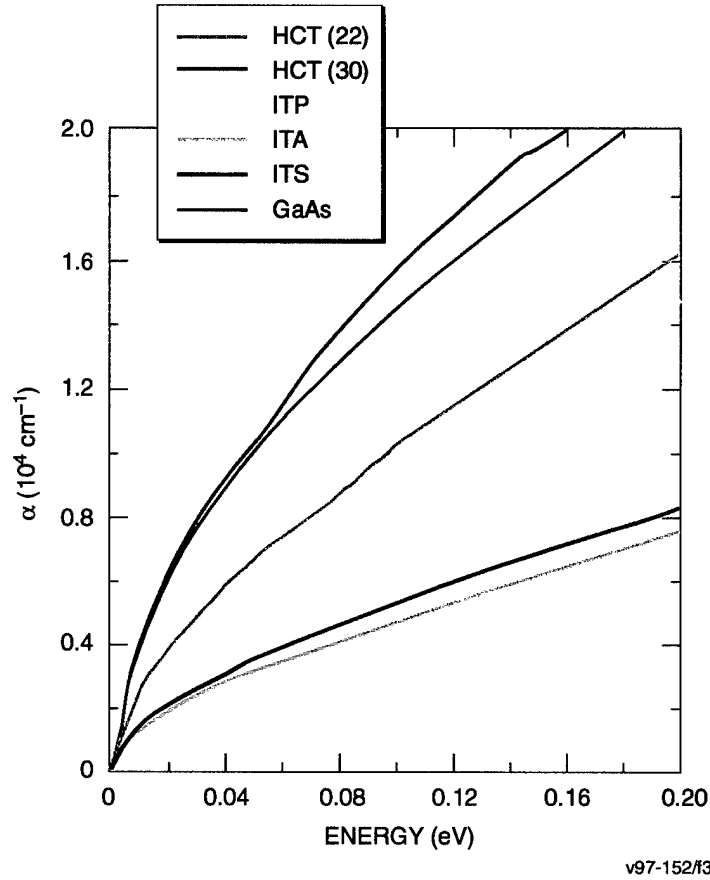
Figure 3 ABSORPTION COEFFICIENTS OF SELECTED COMPOUNDS AND ALLOY. The zero of energy corresponds to the conduction band edge

We have used full-band structures and detailed calculation of matrix elements to obtain the dielectric functions and absorption spectra in GaAs, HgCdTe, InTlP, InTlAs, and InTlSb. The calculations in GaAs, HgCdTe and InTlSb agree reasonably well with the respective experiments. For large gap materials, the absorption coefficient varies approximately $(\hbar\omega - E_g)^{1/2}/\hbar\omega$. However, this functional dependence poorly describes the energy dependence of α in narrow-gap materials. The functional form given by hyperbolic density of states mostly explains the energy dependence. Based on our calculations, we predict that the absorption 0.1 eV gap in InTlP will be nearly as good as that in the GaAs or that in 0.1 eV gap in HgCdTe. This prediction, in addition to other properties of InTlP alloys, makes it a most plausible thallium-based alloy candidate for infrared focal plane array applications.

14

7 DEVICE PROPERTIES—MINORITY CARRIER LIFETIME

The loss of minority carrier by Auger recombination plays an important role in many semiconductor devices such as bipolar transistors, PIN rectifiers, thyristors, and lasers. The efficiency of semiconductor device operations depends on knowledge of the minority carrier lifetime. We set out to make an evaluation of the relative merit of $In_{0.33}Tl_{0.67}P$ and $Hg_{0.78}Cd_{0.22}Te$ with regard to Auger rate.

The Auger recombination is a three-carrier process. In the e–e–h process, an electron in the conduction band recombines with a hole in the valence band. In nonradiative recombination, the released energy is totally absorbed by another electron in the conduction band to reach the excited state. The energy and momentum are conserved. There is also an e–h–h process. However, except in some special cases, this process is insignificant in n-type material because of near-vanishing hole populations at energies well below the top of the valence band edge.

The Auger recombination rate R has been studied considerably. However, all calculations evaluate the required complicated integral in various approximations. The agreement with experiment is usually obtained with a choice of parameters. We demonstrated in a recent publication (Krishnamurthy et al., 1997a) that the calculations with accurate wavefunctions will predict lifetimes about two orders of magnitude longer than experiments in $Hg_{0.78}Cd_{0.22}Te$.

Now we have removed all approximations related to electronic structure and wave-functions. In addition to coulomb scattering, the electron–electron interaction mediated by longitudinal-optical (LO) phonons was also considered (Krishnamurthy et al., 1997b). Additional analysis of these results in terms of overlap integrals and experimental support for hole lifetime dependence on hole density will appear soon (Krishnamurthy et al., 1997c); since another part of this work has not yet appeared in print, the manuscript is included as Appendix B.

The major conclusions of this portion of the study are:

(1) The approximations in wavefunctions can change the calculated lifetimes by 1 to 2 orders of magnitude.

(2) The approximations in the shape and magnitude of valence band structure can change the lifetimes by about an order of magnitude.

(3) The detailed full-bandstructure results agree with experiments in $Hg_{0.78}Cd_{0.22}Te$ within a factor of 2 to 3.

15

(4) With only those holes in a very narrow energy range (typically within 10 meV from the valence band edge) participating in Auger recombination, we show that the hole lifetime is inversely proportional to the hole density in the crystal. The increase in the hole lifetimes with hole density has been observed in GaAs (Ahrenkiel et al., 1991). We further predict a possibility of increasing the minority carrier lifetimes by simply increasing their density outside this narrow energy range.

(5) The minority carrier lifetimes in $In_{0.33}Tl_{0.67}P$ and $In_{0.92}Tl_{0.08}Sb$ are consistently smaller than that in $Hg_{0.78}Cd_{0.22}Te$ under similar conditions. However, the low temperature (77 K) minority carrier lifetimes in $In_{0.85}Tl_{0.15}As$ are an order of magnitude *larger* than that in $Hg_{0.78}Cd_{0.22}Te$. At high temperature, the band gap in $In_{0.85}Tl_{0.15}As$ is much smaller than that in $Hg_{0.78}Cd_{0.22}Te$. Consequently, lifetimes in $Hg_{0.78}Cd_{0.22}Te$ are longer than that in $In_{0.85}Tl_{0.15}As$ at room temperature.

8 EXPERIMENTAL SUPPORT

8.1 MOLECULAR ENERGIES

The phase diagram studies involve the coexistence of the solid and vapor phases. The vapor phase contains two or four phosphorous atoms. As our calculations are related to solid state properties and are obtained in the local density method, we studied the molecular binding energies by the same method.

Using a first-principles method, we have calculated the binding energy of the phosphorous and arsenic dimer and tetramers. The binding energies are summarized in Table 2.

Table 2

MOLECULAR ENERGY IN RYDBERG

Molecule	Energy
P_2	−0.433
P_4	−1.097
As_2	−0.362
As_4	−0.952

Vibrational frequencies of the molecules were also calculated using the first-principles methods. Total energies of the solids InP, InAs, TlP, and TlAs were calculated using the LMTO method and the total energies of the alloys were taken as a weighted average of the constituent compounds. These energies were incorporated into a thermodynamical calculation of the vapor pressure over $In_{1-x}Tl_xP$ and $In_{1-x}Tl_xAs$ as a function of x. For a particular composition x the alloys can exist over a finite range of anion vapor pressures. The anion pressures for the phosphorous-poor side of this existence region were determined by assuming thermodynamical equilibrium with the metals In and Tl. For the alloys, a weighted average of the chemical potentials of the two metals were used. Because of the exceedingly high anion vapor pressures in equilibrium with the thallium-based alloys, all growth efforts have focused on the phosphorous-poor side of the existence region, for which the phosphorous pressures are minimal.

We have examined the As_2 and As_4 partial pressures over $In_{1-x}Tl_xAs$ as a function of composition x and for various temperatures T (Berding et al. (1997). The pressures for InAs $(x = 0)$ are in good agreement with experiment. The upper pressure limit for the GSMBE systems is $\sim 10^{-10}$ atm, and typical growth temperature is ~ 400 °C. From Berding et al. (1997)

17

we see that this corresponds to a composition of $x = 0.3$. We have calculated the P_2 and P_4 pressure over $In_{1-x}Tl_xP$ as a function of x and for various T. The pressures for InP ($x = 0$) are in good agreement with experiment. We find that less than 1% thallium can be obtained by GSMBE.

8.2 EXCHANGE ENERGIES

During the growth of the InTlP alloy, it was observed that the surface layer was rich in Tl, and consequently, formed Tl metal. We hypothesized that Tl in the bulk preferred to exchange its site with the In on the surface. The energy for that exchange is calculated using the Green's function method. The exchange energy is sensitively dependent on the surface on to which the Tl segregates.

First let us look at the exchange of bulk Tl (in TlP) with In in vapor. This involves breaking four TlP bonds and creating four InP bonds. Hence, a simplistic calculation will show that In is favored by about 1.40 eV, which is four times the difference in cohesive energy per bond. The cohesive energy per bond is 1.69 eV in InP and 1.35 eV in TlP. In the cases where the exchange involves a surface atom, the bond counting will yield that n InP bonds and 4 TlP bonds are broken to make n TlP bonds and 4 InP bonds. n is 1, 2, or 3, respectively for (111)B, (100) and (100)A surfaces. In all these cases, Tl is favored on the surface by $(4-n)$ times the difference in the constituent cohesive energies.

We carried out a detailed Green's function calculation that includes the surface charge transfer and the change to the electronic structure due to the exchange. While the overall trend that favors Tl to surface is unchanged, the energetics are considerably different from that obtained in simple bond counting. The Tl is favored on (111)B, (100), and (111)A surfaces by 6, 3, and 2.5 times the difference in cohesive energies of InP and TlP, respectively.

It should be noted that these numbers are meaningful only when they are used in a growth model that takes account of over pressure and entropy in the vapor phase. The reliable information about exchange at finite temperature can be obtained only by minimizing free energy where the system is at equilibrium.

8.3 CONDUCTIVITY

The semimetal TlP is expected to have high conductivity. As our research is toward making devices based in InTlP, we were interested in finding if the conductivity of TlP is comparable to that of the most common interconnects, Al or Cu. If the conductivity is acceptable, TlP or some alloys rich in Tl can be grown along with the active device material. Because the interconnect is grown in the chip, the reduced RC time constant improves the effective speed or efficiency of the device by several orders of magnitude.

We carried out the conductivity calculations based on the Drude model and our band structures. The ratio R of the conductivity of Al to that of TlP is given in Table 3 for various temperatures, doping concentrations, and dopant levels E_D. The E_D is measured from the conduction band edge. We find the best performance is obtained at 77K and doping concentration of 10^{18} cm^{-3} impurities with dopant level at 120 meV in the conduction band. It appears that TlP will be a serious contender for interconnect and its performance could be tailored with the appropriate choices of temperature, dopants, and doping concentration.

Table 3

**RATIO OF CONDUCTIVITY OF A1 TO TlP AT
10^{18} cm^{-3} DOPING CONCENTRATION AND AT
VARIOUS TEMPERATURES (in K) AND AT
DOPANT LEVEL (in meV)**

T	30	90	120
77	340	109	77
300	140	134	128

8.4   SUBSTRATES

As InTlP is a relatively newer alloy, the information about the lattice-matched materials that could be used as a substrate is all important. Assuming that the lattice constant varies linearly in the alloy, the possible substrates that are lattice matched to far IR material $In_{0.33}Tl_{0.15}As$ and medium IR materials $In_{0.43}Tl_{0.57}P$ and $In_{0.92}Tl_{0.08}As$ are given in Table 4. We find that both InTlP and InTlAs have several possible substrates which are alloys. Also note that InTlAs alloys have several compounds that could be used as lattice-matched substrates.

Table 4

THE SUBSTRATES THAT ARE LATTICE MATCHED TO
$In_{0.33}Tl_{0.67}P$ (a = 5.93Å, E_g = 0.1 eV) AND
$In_{0.43}Tl_{0.57}P$ (a = 5.92Å, E_g = 0.25 eV)
(THE SUBSTRATE BAND GAP [E_g] IS IN eV)

$In_{0.33}Tl_{0.67}P$	E_g	$In_{0.43}Tl_{0.57}P$	E_g
$Sn_{47}Si_{53}$	0.492	$Sn_{46}Si_{54}$	0.505
$Sn_{81}C_{19}$	0.507	$Sn_{81}C_{19}$	0.519
$InAs_{32}P_{68}$	1.097	$InAs_{27}P_{73}$	1.150
$Ga_{32}In_{68}As$	0.769	$Ga_{34}In_{66}As$	0.796
$Al_{31}In_{69}As$	1.190	$Al_{33}In_{67}As$	1.240
$AlAs_{41}Sb_{59}$	1.900*	$AlAs_{43}Sb_{57}$	1.910*
$GaAs_{37}Sb_{63}$	1.106	$GaAs_{40}Sb_{60}$	1.121
$AlP_{31}Sb_{69}$	1.800*	$AlP_{32}Sb_{68}$	1.810*
$InP_{90}Sb_{10}$	1.303	$InP_{92}Sb_{08}$	1.322
$GaP_{25}Sb_{75}$	1.370	$GaP_{27}Sb_{73}$	1.410
$CdS_{56}Se_{44}$	2.235	$CdS_{60}Se_{40}$	2.263
$HgS_{73}Se_{27}$	−0.200	$HgS_{77}Se_{23}$	−0.200
$ZnS_{25}Te_{75}$	2.735	$ZnS_{26}Te_{74}$	2.755
$ZnSe_{40}Te_{60}$	2.561	$ZnSe_{42}Te_{58}$	2.571
$CdS_{85}Te_{15}$	2.366	$CdS_{87}Te_{13}$	2.379
$HgS_{90}Te_{10}$	−0.216	$HgS_{92}Te_{08}$	−0.213
$CuCl_{20}I_{80}$	3.170	$CuCl_{21}I_{79}$	3.174
$CuBr_{34}I_{66}$	3.102	$CuBr_{37}I_{63}$	3.101

9 REFERENCES

Ahrenkiel, R.K., B. M. Keyes, and D. J. Dunlavy (1991): *J. Appl. Phys.* **70**, 225.

Ariel, F., V. Gerber, and G. Bahir, S. Krishnamurthy, and A. Sher (1996): *Appl. Phys. Lett.*, **69**.

Berding, M. A., M. van Schilfgaarde, A. Sher, M. J. Antonell, and C. R. Abernathy (1997): *J. Elec. Mater.* **26**, 683.

Chen, A.-B, and A. Sher (1995) *Semiconductor Alloys:* (Plenum, New York), p. 157, Chapter 7 and Appendix 7A.

Harrison, W. A. (1980): *Electronic Structures and the Properties of Solids* (Freeman, San Francisco).

Krisnamurthy, S. and A. Sher (1995) *J. Elec. Mater.* **24**, 641.

Krisnamurthy, S., A.-B. Chen, A. Sher, and M. van Schilfgaarde (1995) *J. Elec. Mater.* **24**, 1121.

Krisnamurthy, S., A.-B. Chen, and A. Sher (1996a) *J. Elec. Mater.* **25**, 1254.

Krisnamurthy, S., A.-B. Chen, and A. Sher (1996b) *J. Appl. Phys.* **80**, 4045.

Krisnamurthy, S., A.-B. Chen, and A. Sher (1997a) *J. Elec. Mater.* **26**, 570.

Krisnamurthy, S., A.-B. Chen, and A. Sher (1997b) *J. Appl. Phys.* **82**, 554.

Krisnamurthy, S., A.-B. Chen, and A. Sher (1997c) *J. Elec. Mater.* (submitted).

Levine, B. J., C. G. Becthea, K. G. Glogvosky, J. W. Stayt, and R. E. Leibenguth (1991): *Semi. Sci. Tech*, **6**, C114.

Osbourn, G. C., L. R. Dawson, R. M. Biefeld, T. E. Zipperian, I. J. Fritz, and B. L. Doyle (1987): *J. Vav. Sci. Tech*, A5, 3150.

Sher, A., M. A. Berding, M. van Schilfgaarde, and A.-B. Chen (1991): *Semicond. Sci. Tech*, **6**, C59–C70.

Sher, A. M. van Schilfgaarde, S. Krishnamurthy, and M. A. Berding (1994): *J. Elec. Mater.*, **24**, 1119.

van Schilfgaarde, M., and A. Sher, (1993): *Appl. Phys. Lett.* **62**, 1857; van Schilfgaarde, M., A.-B. Chen, S. Krishnamurthy, and A. Sher: *Appl. Phys. Lett.* **65**, 2714.

Zelko, J. and J. E. Green (1978): *Appl. Phys. Lett.* **33**, 254.

APPENDIX A

M. A. Berding, "Defects in InTlSb, InTlAs, and InTlP"

Defects in InTlSb, InTlAs, and InTlP

M. A. Berding

SRI International, Menlo Park, California 94025

(August 16, 1996)

$Hg_{0.78}Cd_{0.22}Te$ is currently the dominant material used for high–performance long–wave infrared (LWIR) detectors. Unfortunately, the material is not very robust, and the cation vacancy is a dominant defect, impacting the as–grown carrier type and often making it necessary to perform post–growth and post–processing–step low temperature anneals under high mercury over pressures. The ease with which the cation vacancies form is related to the underlying weakness of the Hg–Te bond. In previous work we have predicted that a new class of alloys which should have band gaps in the LWIR $In_{1-x}Tl_xA$, where A is P, As or Sb, and where $x=0.67$, 0.15, and 0.09 respectively, should have mechanical properties that are superior to the HgCdTe. In this paper we present the results of a preliminary examination of the properties of native defects in the Tl–containing alloys.

Native point defect densities have been calculated for $In_{0.92}Tl_{0.08}Sb$, $In_{0.85}Tl_{0.15}As$, and $In_{0.33}Tl_{0.67}P$. Because of the difficulty in accurately calculating the defect ionization energies in the relatively concentrated alloys, the following analysis will include the neutral defects only. The effect of including the ionized defects into the problem will be only to *increase* the defect populations. Additionally, defects related to In are assumed to be small so that only Tl-defects have been included. Thallium vacancies V_{Tl}, anion vacancies, V_A, thallium antisites Tl_A, and anion antisites A_{Tl}, (where A represents the anion P, As, or Sb) have been included in the analysis; interstitials have not yet been considered.. The approach used is similar to that described in Berding *et al.*; a brief summary is given here.

The following four defect reactions are considered:

$$TlA \rightarrow V_{Tl}A + Tl_g, \qquad (1)$$

$$Tl_g \rightarrow TlV_A, \qquad (2)$$

$$2\text{Tl}_g \rightarrow \text{TlTl}_A, \tag{3}$$

and

$$2\text{Tl}A \rightarrow A_{\text{Tl}}A + 2\text{Tl}_g. \tag{4}$$

Tl_g represents a Tl atom in the gas, which we have chosen to use as our reference state. The anion monomer, dimer or tetramer could have just as well been chosen, with equivalent conclusions reached.

Defect populations are determined in the usual manner from the mass action relations. Again using the Tl partial pressure as the reference, we obtain for the neutral defect concentrations:

$$[V_{\text{Tl}}] = C_0 \left(\frac{2\pi m_{\text{Tl}} k_B T}{\hbar} \right)^{3/2} \left(\frac{k_B T}{P_{\text{Tl}}} \right) \exp \left(\frac{-\Delta F_{V_{\text{Tl}}}}{k_B T} \right), \tag{5}$$

$$[V_A] = C_0 \left(\frac{\hbar}{2\pi m_{\text{Tl}} k_B T} \right)^{3/2} \left(\frac{P_{\text{Tl}}}{k_B T} \right) \exp \left(\frac{-\Delta F_{V_A}}{k_B T} \right), \tag{6}$$

$$[\text{Tl}_A] = C_0 \left(\frac{\hbar}{2\pi m_{\text{Tl}} k_B T} \right)^{3} \left(\frac{P_{\text{Tl}}}{k_B T} \right)^2 \exp \left(\frac{-\Delta F_{\text{Tl}_A}}{k_B T} \right), \tag{7}$$

and

$$[A_{\text{Tl}}] = C_0 \left(\frac{2\pi m_{\text{Tl}} k_B T}{\hbar} \right)^{3} \left(\frac{k_B T}{P_{\text{Tl}}} \right)^2 \exp \left(\frac{-\Delta F_{A_{\text{Tl}}}}{k_B T} \right). \tag{8}$$

The ΔF are the formation free energies for the corresponding reactions in Eqns. (1)-(4), excluding the configuration entropy of the defects (which is using in writing the mass action equations) and the translational free energy of Tl in the vapor phase (which has been explicitly included in the equations); the ΔF include the changes in both the electronic energies and vibration free energies of the reaction. The electronic contributions to ΔF are calculated using the gradient corrected (GC) local density (LD) calculations, which have been shown to give good agreement with experiment when reaction are referenced to a free atom state.[1] The vibration free energies were calculated using a valence force field model for

the lattice and a Green's function method to included the defects.[1] To determine the range of Tl partial pressures that exist over the solid, we must consider the phase diagram of the alloy.

In a stable binary compound such as GaAs, at a given temperature, the compound exists over a finite range of cation and anion partial pressures; we shall refer to this range as the "existence region" or "stablilty region" of the compound. Bounding the existence region is the three phase line, two of which are the compound and the vapor, and at high temperatures the third phase typically being a binary liquid. At a given temperature, defect concentrations will vary across the region, sometimes by many orders of magnitude. Thus to calculate the defect densities, both the temperature and the position in the existence region (as characterized by one of the component chemical potentials or partial pressures) must be specified.

In a stable pseudo-binary alloy such as AlGaAs a similar argument holds, where the liquid with which the alloy is in equilibrium along the three–phase curve is now a ternary liquid. If defect densities are small, it can be shown that even though an additional component is added to the system, the number of degrees of freedom needed to specify the system, as predicted by Gibbs phase rule, does not increase relative to the binary.[2] Thus the temperature and one reference chemical potential (e.g. one component partial pressure) is enough to specify the state of the system in the two phase region.

Because of inherent limitations in the LDA method and the lack of an accurate *ab initio* theory of a ternary liquid, the determination of the existence region of the Tl-based alloys is very difficult.[3] For the purposes of this preliminary defect concentration calculation, we consider a pure Tl–liquid as one phase bounding the zincblende alloy and elemental solid X as another. In each of the three compounds, we find that the Tl partial pressures are comparable when the compound is in equilibrium with these two different solids, thus implying a relatively narrow width for the existence regions.[4] The defects concentrations are calculated for a partial pressure corresponding to equilibration with Tl–liquid, and for pressures up to two orders of magnitude above and below these values to account for inaccuracies in our

calculations, although at present we can not confidently predict that the existence region is within these bounds.

In Fig. 1(a-c) we have plotted the defect concentrations as a function of the Tl partial pressure at 350° C and 450° C. First we note that both the anion and Tl vacancies are negligible in all three compounds. This is in sharp contrast to what is found for $Hg_{0.78}Cd_{0.22}Te$, where the cation vacancy is the dominant defect. Secondly, the anion antisites concentrations are enormously high in some cases; the quantitative values of these predicted high concentrations are unreliable because they are well out of the dilute concentration limit which was assumed in deriving the mass action relations; none the less, the calculations do indicate that the anion antisite density will be quite high and will dominate, except at the highest Tl pressures (or lowest anion pressures) that we have examined, where the thallium antisite begins to dominate. Both the anion and Tl antisite densities are lowest in $In_{0.85}Tl_{0.15}As$, making it favored over the Sb– and P–based alloys in this regard, although even in the As-based alloy antisites might plague the material, considering that their concentrations will be even higher when ionized states are included.

In conclusion we present the results of a preliminary examination of the properties of native defects in $Tl_{0.67}In_{0.33}P$, $Tl_{0.15}In_{0.85}As$, and $Tl_{0.09}In_{0.91}Sb$. We predict that the anion vacancy is the dominant defect and will be most prevalent in the the P–based alloy and least prevalent in the Sb–based alloy. The high P antisite densities are indicative of the formation of the TlP_3 compound in the zincblende–based CuAu structure that we have found elsewhere to have an excess energy comparable to TlP. Several improvements to the calculations must be included before quantitative predictions can be made. (1) The electronic excitation states must be included. This will only increase the defect populations. (2) Cation and anion interstitials must be included in the analysis, but will not impact neutral antisite and vacancy densities presented here. (3) Improved treatment of alloy effects must be included, which we expect will reduce the results presented here by no more than by a factor of ten. (4) Perhaps most importantly, the actual existence region of the alloys must be determined; the complication arises because currently we do not predict the Tl–bearing III-V zincblende

compounds to be stable. We have assumed the alloy is in equilibrium with a pure Tl liquid and looked at defects with Tl pressures about the equilibrium point, but the correct ternary (Tl–In–A) liquid in equilibrium with the growing alloy of concentration x at temperature T must really be included. This improvement to the calculation could dramatically change our results by shifting the equivalent Tl–pressures with which the alloys are in equilibrium. As our predictions of the phase diagrams improve, we will refine our defect calculations accordingly.

REFERENCES

[1] M. A. Berding, M. van Schilfgaarde, and A. Sher, *Phys. Rev. B* **50** 1519 (1994).

[2] R. F. Brebrick, *J. Phys. Chem. Solids* **40** 177 (1978).

[3] We have considered various ways to calculate the properties of the liquid state, but have not yet implimented and tested them against the behavior of known materials.

[4] Depending on the values used for the vibrational free energies, in some cases we find a negative width to the existence region, a consequence of the instability of the TlX compound with respect to decomposition into the elemental constituents.
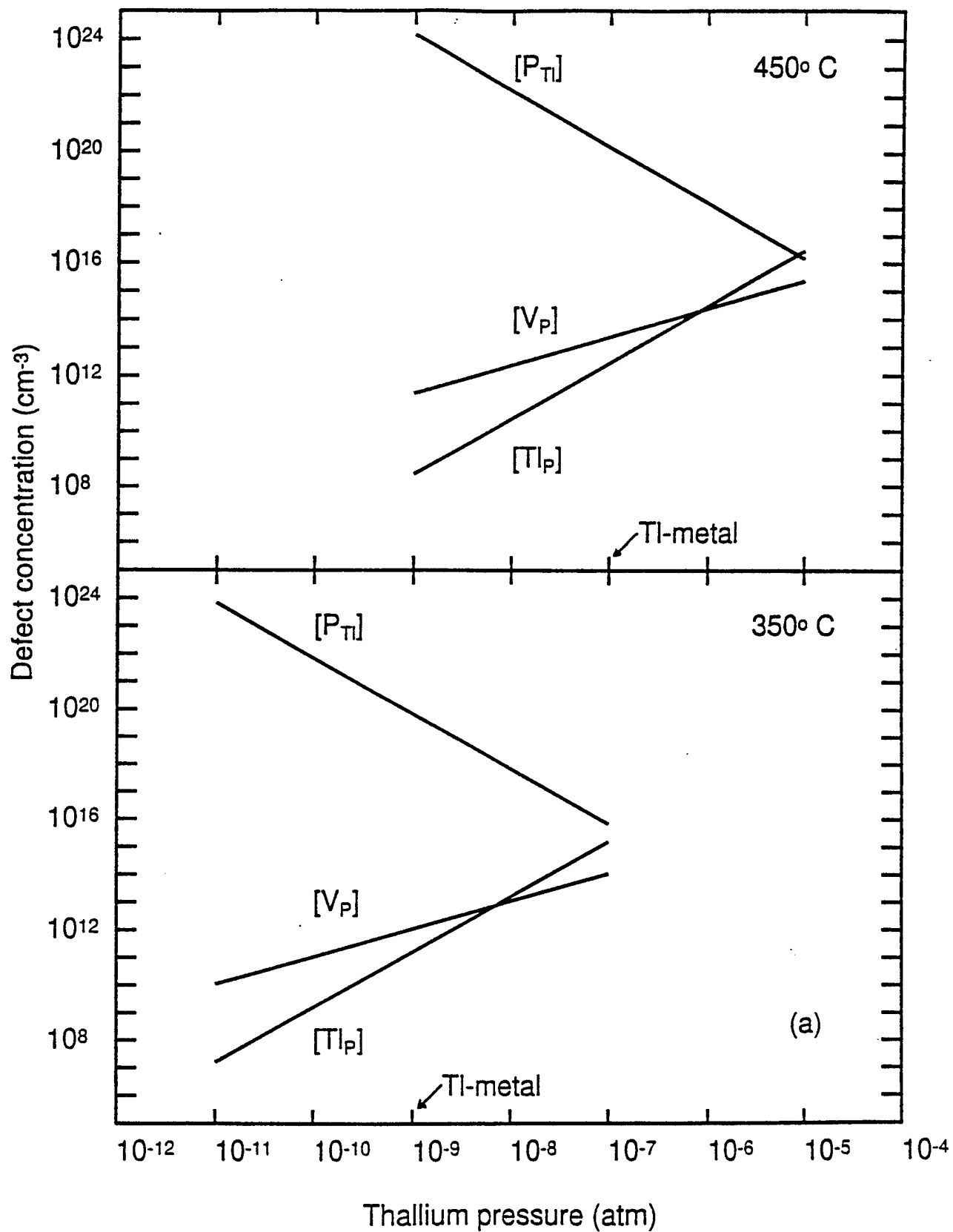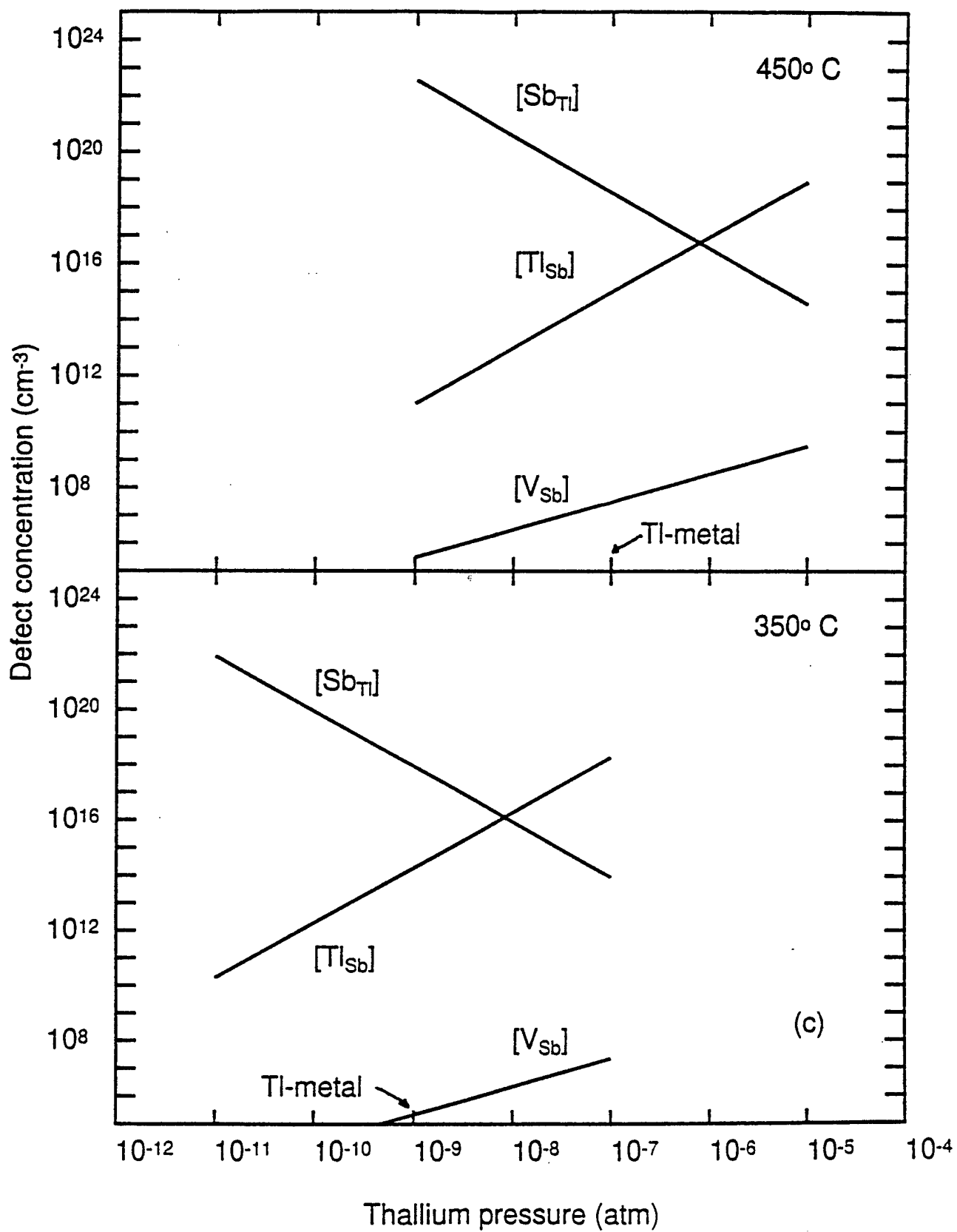
FIG. 1. Neutral native point defect densities as a function of Tl partial pressure in (a) $In_{0.92}Tl_{0.08}Sb$. (b) $In_{0.85}Tl_{0.15}As$, and (c) $In_{0.33}Tl_{0.67}P$.
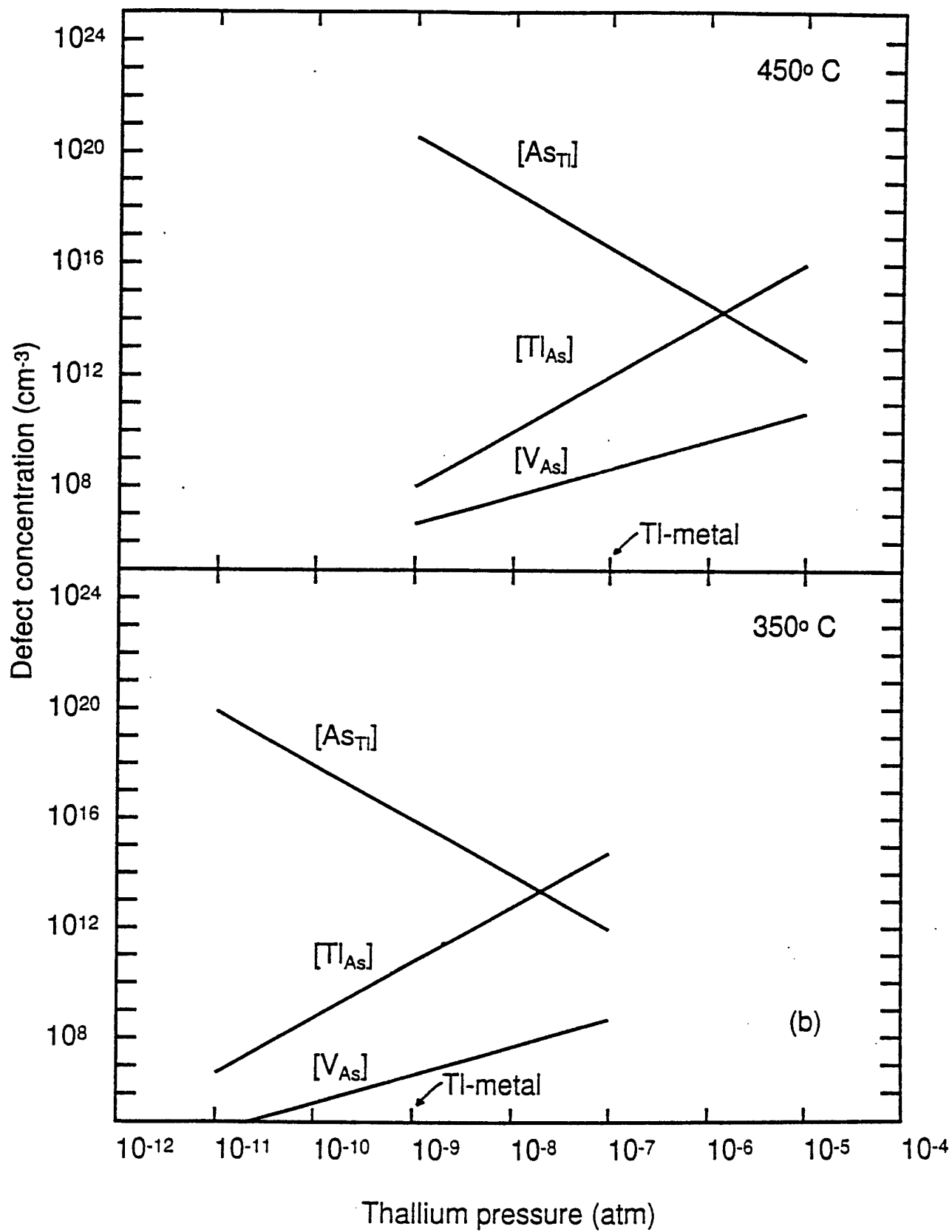
APPENDIX B

S. Krishnamurthy, A.-B Chen, and A. Sher, "Full band structure calculation
of minority carier lifetimes in HgCdTe and thallium-based alloys"

Full band structure calculation of minority carrier lifetimes in HgCdTe and thallium-based alloys

Srinivasan Krishnamurthy,[a] A.-B. Chen,[b] and A. Sher[a]

[a] SRI International, Menlo Park, CA 94025

[b] Physics Department, Auburn University, Auburn, AL 36349

(January 6, 1998)

Abstract

We have calculated the full band structures-based minority carrier lifetimes in small-gap semiconductor alloys. The contribution from first-order Coulomb interactions and second-order electron–electron interactions coupled through optical phonons are included. Our results agree reasonably well with experiments in $Hg_{0.78}Cd_{0.22}Te$. Similar calculations were carried out for lifetimes in $In_{0.67}Tl_{0.33}P$, $In_{0.85}Tl_{0.15}As$, and $In_{0.92}Tl_{0.08}Sb$. The minority carrier lifetimes in $In_{0.67}Tl_{0.33}P$ and $In_{0.92}Tl_{0.08}Sb$ are shorter than that in $Hg_{0.78}Cd_{0.22}Te$ at all temperatures. However, the low-temperature minority carrier lifetime in $In_{0.85}Tl_{0.15}As$ is an order of magnitude longer than that in $Hg_{0.78}Cd_{0.22}Te$. Our calculations further suggest the possibility of increasing the lifetimes of minority carriers either by decreasing the density of states inside a critical energy and momentum region or by increasing the total hole population outside that critical region. Experimental observations that substantiate this suggestion are discussed.

I. INTRODUCTION

The Auger recombination (AR) rate has an important role in semiconductor devices such as bipolar transistors, PIN rectifiers, thyristors, and lasers. The minority carrier lifetime, determined principally by the AR, is used in the evaluation of device efficiency. The AR is a three-carrier process. In the commonly studied electron–electron–hole process, two electrons in conduction band states interact—with one of them combining with a hole in the valence band (VB). The energy released is taken by the second electron to excite it to a higher state. A hole in the VB is destroyed in this process. There is also a hole–hole–electron process. We set out to make an evaluation of the relative merit of long wavelength infrared (LWIR) materials, $In_{0.67}Tl_{0.33}P$, $In_{0.85}Tl_{0.15}As$, $In_{0.92}Tl_{0.08}Sb$, and $Hg_{0.78}Cd_{0.22}Te$ with regard to minority carrier lifetimes.

Since the pioneering paper,[1] the AR rate has been studied extensively in bulk materials,[2] quantum wells,[3] and superlattices.[4] Most calculations consider only Coulomb interactions between electrons. A few calculations[2,5] consider deformation-potential-coupled phonon interactions, but found them to be less important. Because full calculations of the rate are computationally intensive, different authors have employed various degrees of simplifying the combination of approximations— flat valence band, parabolic valence and conduction bands, unit overlap, and overlap given by $\mathbf{k} \cdot \mathbf{p}$. While these methods provided important insight into understanding the physics, and, to some extent, the trends, parameterization is needed to get good agreement with the experiments. In the cases where more accurate pseudopotential wave functions were used in evaluating the overlap integrals, the calculated rates were smaller by about two orders of magnitude than those needed to explain the experiments.[6] In addition, in the absence of enough information to extract the parameters from the experiments, the applicability of these methods to new materials is often questionable.

II. CALCULATIONAL PROCEDURE

We use a hybrid pseudopotential tight-binding (HPTB) approach[7] where the information from first-principles band structures is used to yield an empirical pseudopotential Hamiltonian. The advantages of this method are the availability of the Hamiltonian in tight-binding form and that the localized orbitals are expanded in plane waves. We have used this method to study optical and electronic properties of $Hg_{0.78}Cd_{0.22}Te$, $In_{0.67}Tl_{0.33}P$, $In_{0.85}Tl_{0.15}As$, and $In_{0.92}Tl_{0.08}Sb$ alloys.[8]

We used HPTB band structures and considered both Coulomb and electron–phonon interactions to derive expressions for the AR rate and minority carrier lifetime. Also we made a systematic study of the effect of various approximations on the AR, the details of which will be published elsewhere.[9] In this article, we briefly describe our method and discuss the major findings related to minority carrier lifetimes in infrared (IR) materials. We find that the full band structures must be used in the calculation of Fermi levels and wave functions to get reasonable and parameter-free agreement with the experiments. Of the three thallium-based IR materials considered, the 77 K hole lifetimes are larger only in $In_{0.85}Tl_{0.15}As$ than those in $Hg_{0.78}Cd_{0.22}Te$. We further find the hole lifetimes can be increased by designing alloys with either a decreased density of states (DOS) inside an energy range centered about 5 meV below the valence edge that is set by energy and momentum conservation conditions, or by an increased hole population outside that critical region.

In our HPTB method, the localized basis orbitals are expanded in plane waves (about 150) and the matrix elements are calculated between the plane waves. Hence, any Bloch state $|k>$ can also be expanded in a finite number of plane waves:

$$|k> = \frac{1}{\Omega^{1/2}} \sum_{G} A(k+G)e^{i(k+G)\cdot r} \tag{1}$$

where Ω is the crystal volume and G is the reciprocal lattice vector. The AR can be considered as the scattering of two conduction band electrons from their initial states k_1 and k_2 to their final states k_3 and k_4 in the valence and conduction bands, respectively.

The Auger rate R for this scattering is calculated from second-order perturbation theory and the golden rule. After some algebraic manipulation, the AR rate $R(\mathbf{k_3})$ for a hole at $\mathbf{k_3}$ is found to be proportional to the integral,[9]

$$
\begin{aligned}
I &= \int d^3\mathbf{k_2} \int d^3\mathbf{k_1} |F(\lambda) + \zeta F(0)|^2 \\
&\quad \delta(E_{\mathbf{k_1}} + E_{\mathbf{k_2}} - E_{\mathbf{k_3}} - E_{\mathbf{k_1}+\mathbf{k_2}-\mathbf{k_3}}) \\
&\quad f(E_{\mathbf{k_1}}) f(E_{\mathbf{k_2}})(1 - f(E_{\mathbf{k_1}+\mathbf{k_2}-\mathbf{k_3}}))
\end{aligned}
\tag{2}
$$

$$
\zeta = \left[\frac{2(\hbar\omega_L)^2}{E_g^2 - (\hbar\omega_L)^2} \frac{2\pi\kappa_0}{\epsilon_0} \left(\frac{1}{\kappa_\infty} - \frac{1}{\kappa_0} \right) \right]
$$

$$
\begin{aligned}
F(\lambda) = \sum_{\mathbf{G}} &\left[|\mathbf{k_2} - \mathbf{k_4} + \mathbf{G}|^2 + \lambda^2 \right]^{-1} \\
&\left[\sum_{\mathbf{G_1}} A(\mathbf{k_1} + \mathbf{G_1}) A^*(\mathbf{k_1} + \mathbf{k_2} - \mathbf{k_4} + \mathbf{G_1} + \mathbf{G}) \right] \\
&\left[\sum_{\mathbf{G_2}} A(\mathbf{k_2} + \mathbf{G_2}) A^*(\mathbf{k_4} + \mathbf{G_2} - \mathbf{G}) \right]
\end{aligned}
$$

where ω is the phonon frequency; λ^{-1} is the Debye screening length; κ_0 and κ_∞ are zero and infinite frequency dielectric constants, respectively; f is the Fermi-Dirac distribution function; and E_g and $E_\mathbf{k}$ are the band gap and the band energy at wave vector $\mathbf{k}$, respectively. When the electron recombines with the hole in the VB, that hole is considered to be lost. However, the thermalization rate is about three orders of magnitude faster than the Auger rate. Hence, those states emptied by the Auger process are quickly refilled with holes by thermalization. Under these conditions, we showed[9] that the minority carrier lifetime τ_A as measured from photoconductive experiments[10] takes the form

$$
\tau_A = \frac{\sum_{\mathbf{k_3}} e^{\beta E_{\mathbf{k_3}}}}{\sum_{\mathbf{k_3}} e^{\beta E_{\mathbf{k_3}}} R(\mathbf{k_3})},
\tag{3}
$$

where $E_{\mathbf{k_3}}$ is the energy of a hole in momentum state $\mathbf{k_3}$ and $\beta = 1/kT$. Note that this expression for lifetimes does not depend on the hole population.

The quantity ζ is a measure of the relative importance of virtual phonon mediated electron–electron interactions to normal Coulomb (virtual photon mediated) interactions.

If we assume $F(\lambda)$ is independent of λ (which is nearly true[2]), then the rate changes by a factor of $(1+\zeta)^2$. For example, ζ is about 0.15 for 77 K $Hg_{0.78}Cd_{0.22}Te$ and, hence, the extra interaction decreases the lifetime by about 30%. A similar correction is calculated for all thallium alloys considered. We note that ζ is inversely proportional to the band gap. Consequently, the effect of this phonon term is largest at low temperature in $Hg_{0.78}Cd_{0.22}Te$, and equally large at all temperatures in thallium alloys where the gaps remain the same (or decrease) with temperature.

III. RESULTS

We use these expressions to calculate the rates and lifetimes of various IR materials. In all the calculations reported here, energy gap and conduction band structure variation with temperature are used. The crux of the problem is to evaluate time-consuming Eq. (2). Two kinds of approximations are normally used— one related to wave function and the other to hole energy. First, using a flat valence band approximation (FVBA) to evaluate I, we show, in Fig. 1, the lifetimes in $Hg_{0.78}Cd_{0.22}Te$ calculated with wave function given by plane waves (thin dotted line), $k \cdot p$ [11] (thick dotted line), and our HPTB band structures (thin solid line). Then, the full band structure results, (thick solid line) in Fig. 1, where the anisotropic hole energy is also obtained from the HPTB band structure, are calculated and compared with results from experiment[10] (dashed line). In all cases, the experimentally determined n-doping concentration of 1.3×10^{15} cm^{-3} is used, the donor level is taken to resonate at the bottom of the conduction band, and the Fermi levels are calculated using full temperature-dependent band structures.

We see that the lifetimes calculated with wave functions given by plane waves and $k \cdot p$ wave functions are nearly the same and are an order of magnitude *shorter*, and the lifetime obtained from the HPTB band structure (but with FVBA for energy) is an order of magnitude *longer*, than the measured values. This is easily understood from the overlap integrals shown in Fig. 2 as functions of electron wave vector that satisfy the energy and

momentum conservation condition. The wave vector value of 0.05 (2 π/a) corresponds to an energy of 300 meV from the conduction band edge (CBE). The states for wave vectors larger than those shown in Fig. 2 do not contribute to the Auger rate. We see that the (absolute value of the) overlap between the wave function at the valence band edge (VBE) and the wave function at various values of k_1 in the conduction band (solid line) is less than 0.4. The wave functions near the VBE have anion p-symmetry whereas the wave function near the bottom of the conduction band has cation-s symmetry. The overlap between these wave functions is identically zero when k_1 and k_3 are at the band edges. For wave vectors away from the conduction band edge, the overlap is non zero, but is very small as can be seen in Fig. 2. Similarly, the overlap between the wave function at CBE (k_3) and those at various values of k_4 in the conduction band (dashed line) is between 0.9 and 1. Consequently, the product (dotted line) of the two overlaps is less than 0.3. Hence, the matrix element, where this product enters squared, is reduced by at least a factor of 10. However, because k_1 is more likely to be near the CBE, the matrix element is reduced further (due to reduction in the overlap), thus leaving the lifetimes longer by the same factor. Hence the lifetime values, calculated with FVBA but with accurate wave functions, are two orders of magnitude longer than the plane wave approximation where the overlap is assumed to be unity. However, when the FVBA is removed and the lifetimes are calculated with full band structures, the values (thick solid line in Fig. 1) are reduced by a factor of about 3 and are comparable to the experimental results.[10] In most cases, calculated values are about a factor of 3 larger than experimental values for a wide temperature range. This agreement between parameter-free calculations and the experiment is considered to be good because of the uncertainty in numerical values such as dopant concentration, and the location of donor levels, the band gap and their temperature dependence. For example, a 2 meV error in the band gap can change the calculated lifetimes by 30% at 77 K. Also, uncertainty in experimental estimation of Hg and dopant concentration can alter the agreement. If the dopant concentration is increased from 1.3 to 2.0 $\times$ 10^{15} cm^{-3} or the donor level is moved into the conduction band by 10

meV, the experimental results fall within the calculated range for most temperatures.[9]

We consider anisotropic VB structure in our calculations. The calculated AR rate for hole wave vector directions (in (100) and its adjacent direction are plotted in Fig. 3 as a function of hole energy. The final AR rate is the hole-population-weighted-average of the plotted rate integrated over all directions in the Brillouin Zone. We see that most contributions to the total rate (denominator of Eq. 3) come only from states about 10 meV from the VBE. Even though there are considerable hole populations outside this energy range, the energy and momentum conservation conditions (in Eq. 2) cause the AR rate for those holes to be nearly zero. However, the numerator of Eq. 3 is proportional to the total DOS. Hence, the lifetimes of holes can be increased by increasing the ratio of total DOS to the DOS in this 10 meV energy range. For example, by applying biaxial stress/strain, the degeneracy of the top VB is lifted. If the split-off bands are separated by more than 10 meV, the DOS within that 10 meV is reduced by a factor of 2 and, consequently, the hole lifetimes are increased by about the same factor.

The suppression of Auger recombination in strained materials has been observed.[12] Notice that the reduction suggested by calculations is caused not by the change in the curvature or inversion of the light and heavy hole valance band,[13] but by the restriction of energy and momentum conservation. This is akin to the suggestion made by Grein et al.[4] to choose superlattices for increased minority carrier lifetimes. In addition, because the contributions to the AR come only from a small portion of the band structure near the VBE, the holes created beyond this energy range will live longer, and thus make the average lifetime of the holes also longer. This observation suggests that minority carrier lifetimes increase with the minority carrier population beyond a critical density. This is in agreement with experiment[14] where minority carrier lifetimes increase with incident light intensity in GaAs.

We calculate the rate and hole lifetimes in the 1.3×10^{15} cm^{-3} n-doped IR (0.1 eV gap) materials In$_{0.67}$Tl$_{0.33}$P, In$_{0.85}$Tl$_{0.15}$As, and In$_{0.92}$Tl$_{0.08}$Sb. In all the cases, full band structures with their temperature dependence are considered. The electron–electron interactions

V. ACKNOWLEDGMENTS

mediated by Coulomb and phonons are taken into account. The donor levels are assumed to be at the bottom of the conduction band at any temperature.
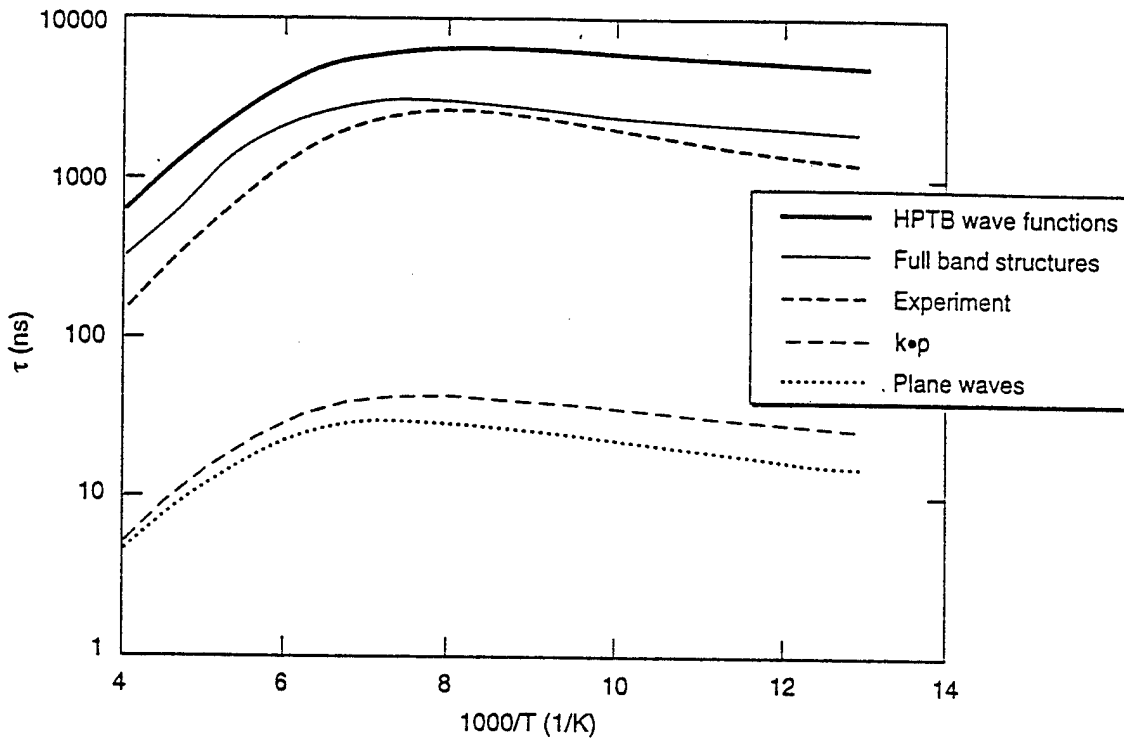
The calculated lifetimes as a function of temperature are compared with $Hg_{0.78}Cd_{0.22}Te$ in Fig. 4. At low temperatures, the hole lifetimes in $In_{0.85}Tl_{0.15}As$ are longer than those in $Hg_{0.78}Cd_{0.22}Te$ by about an order of magnitude. The lifetimes in $In_{0.67}Tl_{0.33}P$ and $In_{0.92}Tl_{0.08}Sb$ are shorter than those in $Hg_{0.78}Cd_{0.22}Te$. For the same band gap, doping concentration, and donor level, we found that $R(k_3)$ at 77 K in $In_{0.85}Tl_{0.15}As$ is one and two orders of magnitude smaller than that in $Hg_{0.78}Cd_{0.22}Te$ and $In_{0.67}Tl_{0.33}P$, respectively. With the effect of DOS nearly canceling out in Eq. 3, lifetimes in $In_{0.85}Tl_{0.15}As$ are correspondingly larger than those in $Hg_{0.78}Cd_{0.22}Te$ and $In_{0.67}Tl_{0.33}P$. At higher temperatures the band gap in $Hg_{0.78}Cd_{0.22}Te$ increases and this reduces the Auger rate substantially. The band gap in $In_{0.67}Tl_{0.33}P$ is nearly independent of temperature; the band gaps in $In_{0.92}Tl_{0.08}Sb$ and in $In_{0.85}Tl_{0.15}As$ *decrease* with temperature. The Auger rate increases and the lifetimes are reduced.

IV. CONCLUSION

We have calculated the Auger rate with wave functions and electronic energy obtained from full band structures. The electron–electron interaction mediated by Coulomb interactions and by phonons are considered. The phonon mediated interaction contributes about 30% at 77 K to the total rate. The theory agrees with one experiment on $Hg_{0.78}Cd_{0.22}Te$ within a factor of 3. The calculated results are within experimental and theoretical uncertainties in various physical parameters. The lifetimes calculations indicate that $In_{0.85}Tl_{0.15}As$ will be preferred to $Hg_{0.78}Cd_{0.22}Te$ at low temperatures. Hole lifetimes in $Hg_{0.78}Cd_{0.22}Te$ are longer than those in $In_{0.67}Tl_{0.33}P$ or $In_{0.92}Tl_{0.08}Sb$. However, an important conclusion is that the hole lifetimes could be increased either by designing alloys that appropriately modify the valence band structure inside a specified energy range or by increasing the hole density outside that energy range.

REFERENCES

[1] A.R. Beattie and P.T. Landsberg, Proc. of Royal Soc., **A 249**, 16 (1958).

[2] A. Haug, J. Phys. C, **16**, 4159 (1983); J. Phys. Chem. Solids, **49**, 599 (1988) and references cited therein.

[3] A. Haug, Semicond. Sci. Tech. **7**, 1337 (1992).

[4] C.H. Grein, P.M. Young, and H. Ehrenreich, J. Appl. Phys. **76**, 1940 (1994).

[5] W. Lochmann, Phys. Status Solidi a **42**, 181 (1977).

[6] M.G. Burt, S. Brand, C. Smith, and R.A. Abraham, J. Phys. C, **17**, 6385 (1984).

[7] A.-B. Chen and A. Sher, *Semiconductor Alloys* (Plenum, New York), p. 157, Chapter 7 and Appendix 7A (1995).

[8] S. Krishnamurthy, A.-B. Chen, and A. Sher, J. Elec. Mater. **26**(6), 570 (1997).

[9] S. Krishnamurthy, A.-B. Chen, and A. Sher, J. Appl. Phys. **82**, 5540 (1997). 1997).

[10] M.C. Chen and L. Colombo, J. Appl. Phys. **72**, 4761 (1992).

[11] B.K. Ridley, *Quantum Processes in Semiconductors* (Clarendon, Oxford), p. 269 (1982).

[12] Y. Zou, J.S. Osinski, P. Grodzinski, P. Dapkus, W.C. Rideout, W.F. Sharfin, J. Schlafer, and F.D. Crawford, IEEE J. of Q. Elec. **29** 1565 (1993).

[13] A.R. Adams, Electron Lett., **22**, 249 (1986).

[14] R.K. Ahrenkiel, B.M. Keyes, and D.J. Dunlavy, J. Appl. Phys. **70**, 224 (1991).

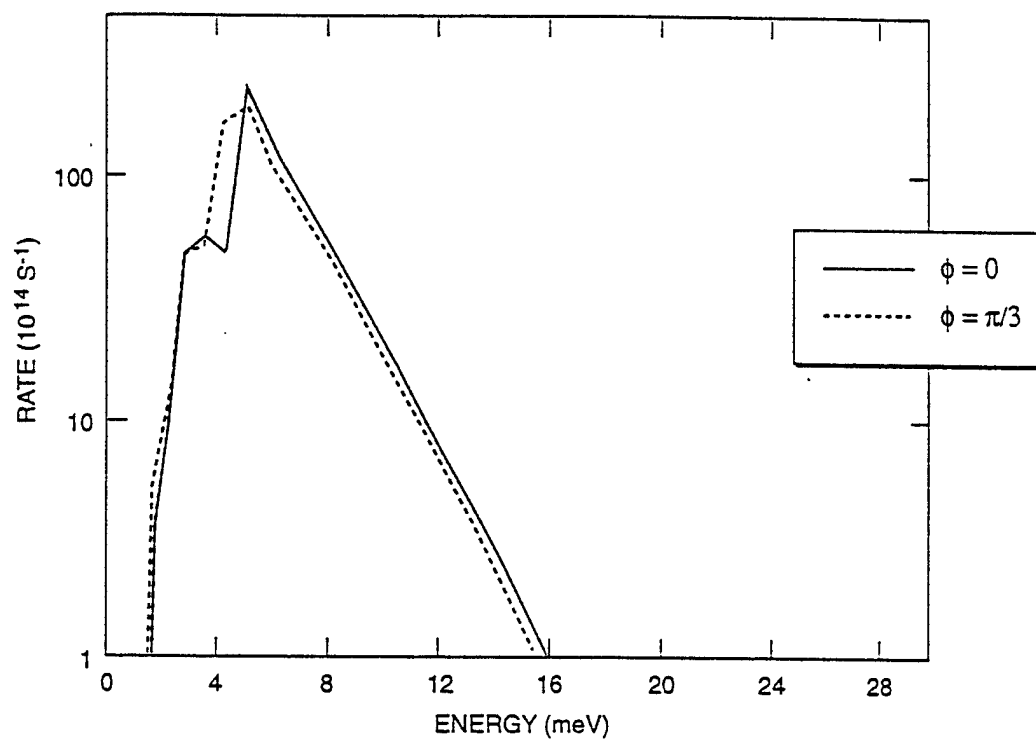FIG. 1. Auger lifetimes in $Hg_{0.78}Cd_{0.22}Te$ calculated using flat valence band and overlap obtained from plane waves, $k \cdot p$ and HPTB band structure wave functions. The full band structure results and experimental values are given.
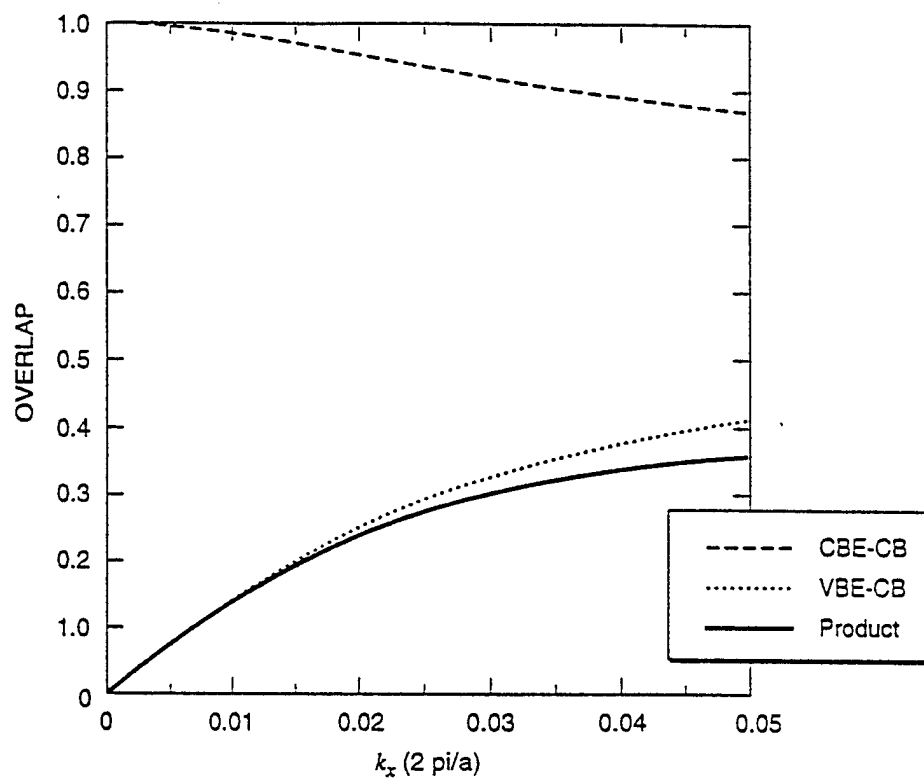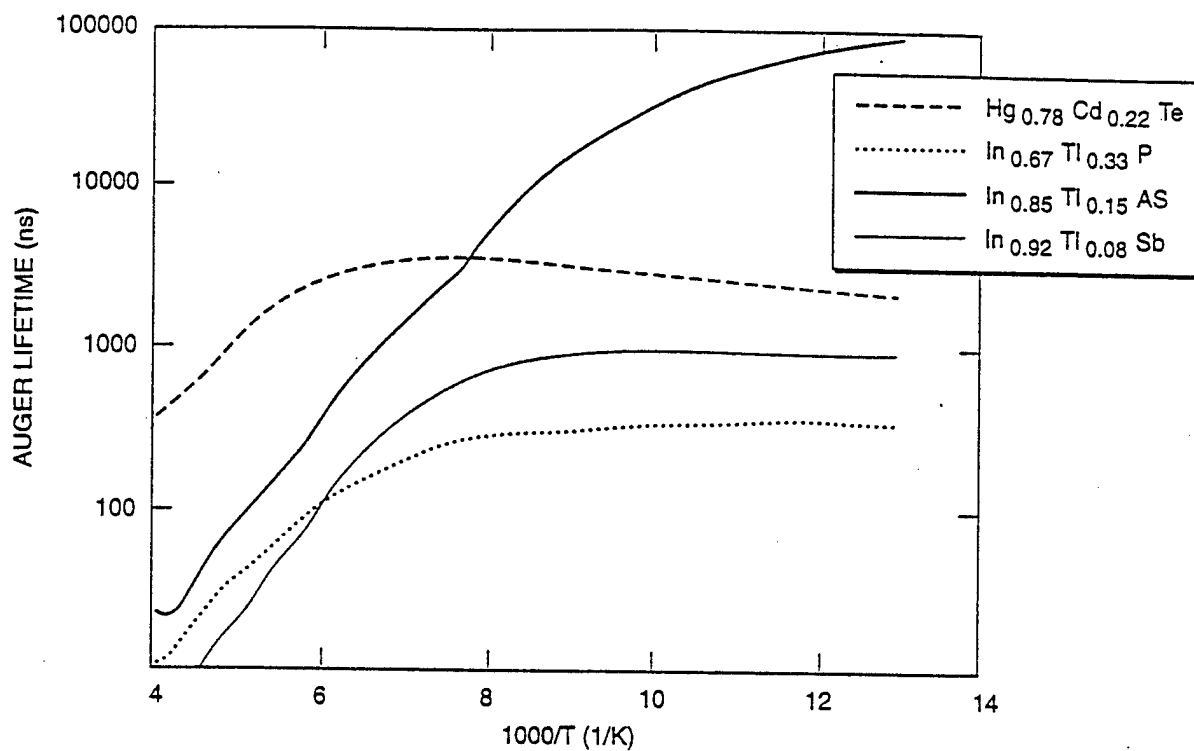
FIG. 2. Overlap in $Hg_{0.78}Cd_{0.22}Te$ between wave function at the VBE and that at various k in the conduction band, between wave function at the CBE and that at various k in the conduction band, and the product of these overlaps.

FIG. 3. Calculated Auger rates in $Hg_{0.78}Cd_{0.22}Te$ in (100) and adjacent direction to (100) as a function of hole energy (in meV from VBE).

v97-119/f3

FIG. 4. Calculated lifetimes in $Hg_{0.78}Cd_{0.22}Te$, $In_{0.67}Tl_{0.33}P$, $In_{0.85}Tl_{0.15}As$ and $In_{0.92}Tl_{0.08}Sb$. All materials have a gap of 102 meV at 77 K.